Molecular Cell

Article

TIRR inhibits the 53BP1-p53 complex to alter cell-fate programs

Graphical abstract

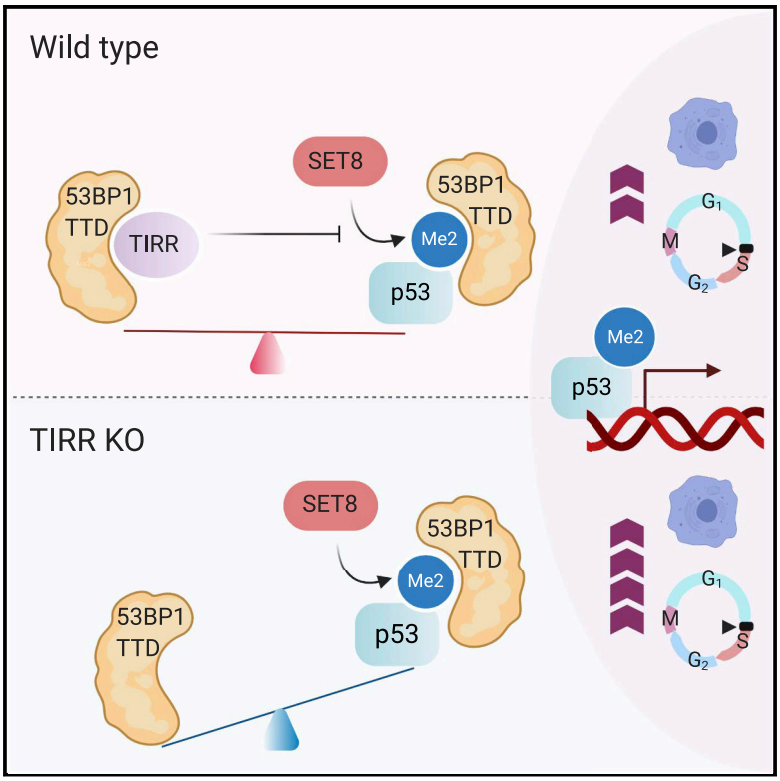

Authors

Nishita Parnandi, Veronica Rendo, Gaofeng Cui, ..., Matthias Altmeyer, Georges Mer, Dipanjan Chowdhury

Correspondence

dipanjan_chowdhury@dfci.harvard.edu

In brief

Parnandi et al. demonstrate that the Tudor interacting repair regulator (TIRR) protein impacts 53BP1 functions beyond DNA repair. TIRR inhibits 53BP1-mediated p53 gene transactivation, and consequently affects cell fate. Mechanistically, TIRR competes with p53 for the Tudor domain of 53BP1. Furthermore, TIRR inhibits p53 signaling in breast and prostate cancers.

Highlights

- TIRR deficiency hyperactivates 53BP1-mediated p53 gene transactivation
- TIRR loss alters p53-dependent cell-fate programs, including survival and senescence
- TIRR inhibits the complex formation between 53BP1-Tudor and dimethylated p53 (K382me2)
- p53-proficient tumors are likely to maintain stable TIRR expression

Parnandi et al., 2021, Molecular Cell *81*, 1–13
June 17, 2021
https://doi.org/10.1016/j.molcel.2021.03.039

CellPress

Please cite this article in press as: Parnandi et al., TIRR inhibits the 53BP1-p53 complex to alter cell-fate programs, Molecular Cell (2021), https://doi.org/10.1016/j.molcel.2021.03.039

Molecular Cell

CellPress

Article

TIRR inhibits the 53BP1-p53 complex to alter cell-fate programs

Nishita Parnandi,[1,2] Veronica Rendo,[3,4,5,6] Gaofeng Cui,[7] Maria Victoria Botuyan,[7] Michaela Remisova,[8] Huy Nguyen,[1] Pascal Drané,[1] Rameen Beroukhim,[3,4,5,6] Matthias Altmeyer,[8] Georges Mer,[7] and Dipanjan Chowdhury[1,2,6,9,*]

[1]Department of Radiation Oncology, Dana-Farber Cancer Institute, Boston, MA 02115, USA
[2]Department of Biological Chemistry & Molecular Pharmacology, Harvard Medical School, Boston, MA 02115, USA
[3]Department of Medical Oncology, Dana-Farber Cancer Institute, 450 Brookline Avenue, Boston, MA 02215, USA
[4]Cancer Program, Broad Institute, 415 Main Street, Cambridge, MA 02142, USA
[5]Department of Medicine, Harvard Medical School, 25 Shattuck Street, Boston, MA 02115, USA
[6]Broad Institute of Harvard and MIT, Cambridge, MA 02142, USA
[7]Department of Biochemistry and Molecular Biology, Mayo Clinic, Rochester, MN 55905, USA
[8]Department of Molecular Mechanisms of Disease, University of Zurich, Zurich, Switzerland
[9]Lead contact
*Correspondence: dipanjan_chowdhury@dfci.harvard.edu
https://doi.org/10.1016/j.molcel.2021.03.039

SUMMARY

53BP1 influences genome stability via two independent mechanisms: (1) regulating DNA double-strand break (DSB) repair and (2) enhancing p53 activity. We discovered a protein, Tudor-interacting repair regulator (TIRR), that associates with the 53BP1 Tudor domain and prevents its recruitment to DSBs. Here, we elucidate how TIRR affects 53BP1 function beyond its recruitment to DSBs and biochemically links the two distinct roles of 53BP1. Loss of TIRR causes an aberrant increase in the gene transactivation function of p53, affecting several p53-mediated cell-fate programs. TIRR inhibits the complex formation between the Tudor domain of 53BP1 and a dimethylated form of p53 (K382me2) that is poised for transcriptional activation of its target genes. TIRR mRNA expression levels negatively correlate with the expression of key p53 target genes in breast and prostate cancers. Further, TIRR loss is selectively not tolerated in p53-proficient tumors. Therefore, we establish that TIRR is an important inhibitor of the 53BP1-p53 complex.

INTRODUCTION

The p53-binding protein 1 (53BP1) is pivotal in maintaining the balance of competing DNA double-strand break (DSB) repair pathways, which is crucial for genomic stability (Chapman et al., 2012; Zimmermann and de Lange, 2014). The function of 53BP1 beyond DSB repair has recently emerged in the context of its interaction with p53 (Durocher and Pelletier, 2016). Perturbing "normal" mitosis caused a p53-dependent cell-cycle arrest, which was shown to be dependent on 53BP1 and its known interactor USP28 (Fong et al., 2016; Lambrus et al., 2016; Meitinger et al., 2016). The proposed mechanism was that 53BP1 stabilizes p53 protein levels. A parallel study reported that ionizing radiation (IR) or Nutlin-3 treatment of 53BP1-deficient cells did not alter p53 protein levels but significantly diminished the transcriptional activation of several p53 target genes, including cell-cycle (*CDKN1A/p21*), auto-regulatory (*MDM2*), and pro-apoptotic (*BAX*, *PUMA/BBC3*) genes (Cuella-Martin et al., 2016). This p53-mediated transactivation was mediated by the tandem-BRCT domain of 53BP1. However, structural studies have revealed that two independent domains of 53BP1 (tandem Tudor and tandem BRCT, referred to as Tudor and BRCT hereafter) directly bind p53 with comparable affinity (Derbyshire et al., 2002; Joo et al., 2002, Roy et al., 2010; Tong et al., 2015). The role of Tudor, in the context of p53 transactivation, remained unclear. These studies emphasized the importance of 53BP1 in p53 function and highlighted the fundamental gap in our knowledge regarding the molecular mechanism and physiological relevance of 53BP1-mediated regulation of p53.

We and others recently identified TIRR (Tudor-interacting repair regulator) as a direct interactor and regulator of 53BP1 function in DSB repair (Drané et al., 2017; Zhang et al., 2017). 53BP1 recruitment to DSBs by the recognition of histone H4 dimethylated at lysine K20 (H4K20me2) is inhibited by TIRR binding to the Tudor of 53BP1 (Botuyan et al., 2018; Dai et al., 2018; Wang et al., 2018). An important yet unanswered question is whether TIRR affects the functions of 53BP1 that are not reliant upon its recruitment to DSBs. Here, we show that the loss of endogenous TIRR causes an aberrant increase in p53-mediated gene transactivation under different conditions of cellular stress. Phenotypically, TIRR deficiency results in decreased cell survival, higher senescence, and an increase in

Please cite this article in press as: Parnandi et al., TIRR inhibits the 53BP1-p53 complex to alter cell-fate programs, Molecular Cell (2021), https://doi.org/10.1016/j.molcel.2021.03.039

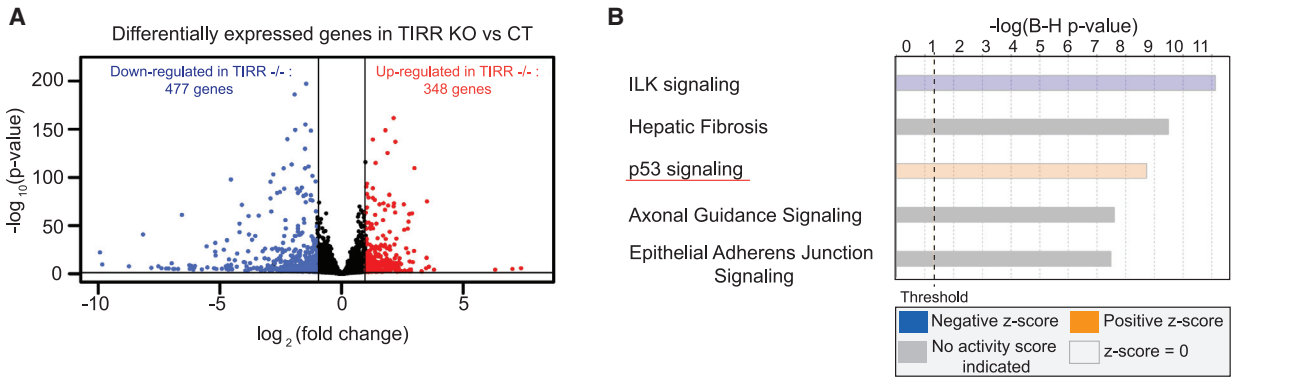

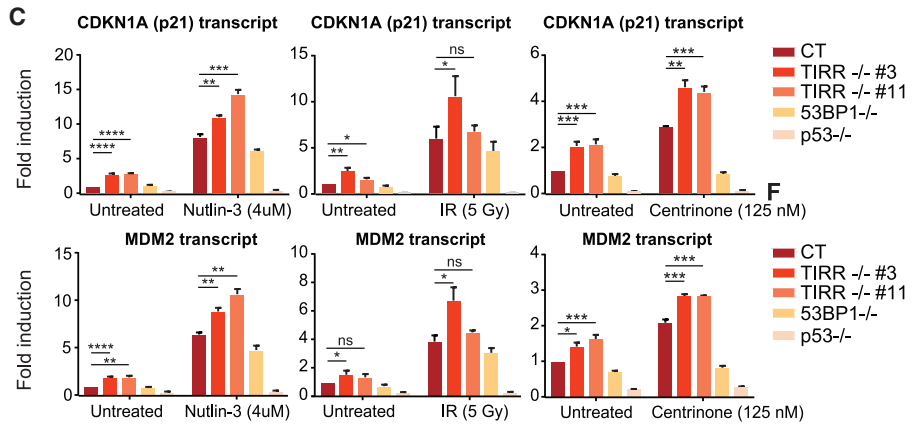

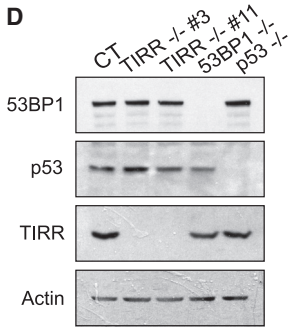

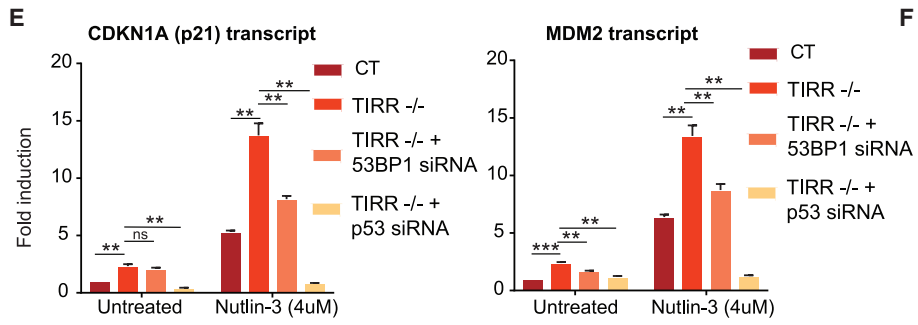

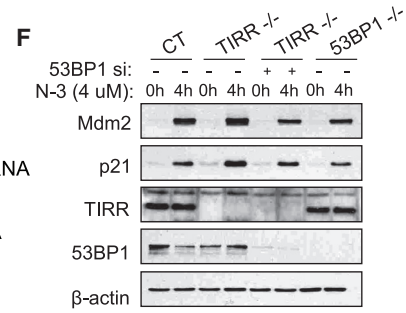

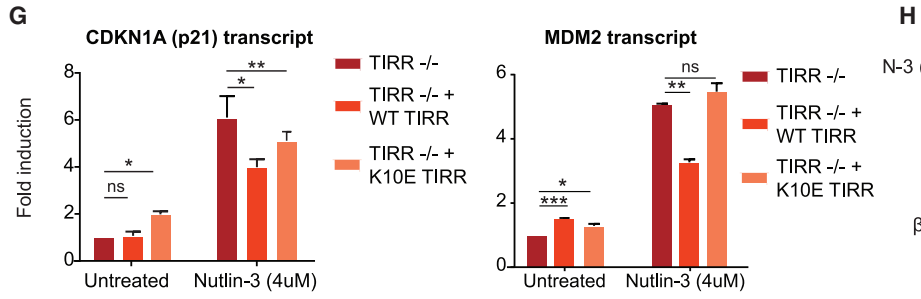

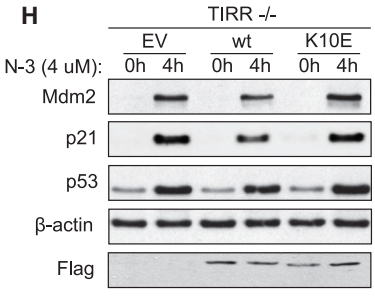

(legend on next page)

Please cite this article in press as: Parnandi et al., TIRR inhibits the 53BP1-p53 complex to alter cell-fate programs, Molecular Cell (2021), https://doi.org/10.1016/j.molcel.2021.03.039

CDKN1A(p21)-mediated checkpoint arrest. From a mechanistic standpoint, TIRR modulates the stress-induced interaction of 53BP1 and p53. Using nuclear magnetic resonance (NMR) spectroscopy, we demonstrate that TIRR competes with p53 dimethylated at residue K382 (p53K382me2) for the Tudor domain of 53BP1. We further show that the impact of TIRR on p53 is specifically dependent on SET8-mediated methylation of p53. Analysis of cancer genomes reveals that high *TIRR* expression levels negatively correlate with the expression of key p53 targets, thereby mimicking diminished p53 activity. Furthermore, amplifications of the *TIRR* genomic locus were mutually exclusive from *TP53* mutations/deletions and amplifications of the *MDM2/4* loci, suggesting that these are distinct mechanisms of suppressing p53 function in human cancers. Thus, we report for the first time the significance of TIRR as an upstream inhibitor of the 53BP1-p53 complex.

RESULTS

TIRR loss increases 53BP1-dependent gene transactivation property of p53

To identify the cellular pathways that are influenced by TIRR, we analyzed gene expression by bulk RNA sequencing (RNA-seq) in 2 clones of the U2OS TIRR-knockout (KO) cell line. Relative to control, the loss of TIRR resulted in the increased expression of 348 genes ($\log_2$ fold change > 1) and decreased expression of 477 genes ($\log_2$ fold change < −1) (Figure 1A). Gene annotation and pathway analysis revealed that the p53 pathway was one of the statistically top-ranked pathways that were upregulated in TIRR-KO cells ($p < 0.005$) (Figure 1B). To validate this result and further analyze the p53 pathway in the context of exogenous activation (via Nutlin-3 treatment), the expression of 92 p53 pathway genes comprising upstream activators, downstream transcriptional targets, and co-activators was examined by qRT-PCR in control and TIRR-KO cells (Figure S1A). Only p53 transcriptional transcripts were significantly upregulated in both untreated and Nutlin-3-treated TIRR-KO cells. Next, we used a subset of p53 target genes, *CDKN1A (p21)*, *MDM2*, *BAX*, and *BBC3/PUMA*, as a readout of p53 activity, to examine the impact of TIRR in the context of different stress signals (Nutlin-3, IR, and Centrinone [PLK-4 inhibitor]). The loss of TIRR caused a consistent increase in p53-target gene transcripts independent of the mode of p53 activation (Figures 1C, 1D, S1B, and S1C). Since the loss of TIRR affects 53BP1-mediated DNA repair functions, we investigated whether TIRR-KO cells harbor increased endogenous DNA damage that could activate p53. However, there was no significant increase in γ-H2AX levels in untreated or Nutlin-3-treated TIRR-KO cells (Figure S1D). To further address whether DNA damage-induced signaling is involved in the enhanced p53 response in TIRR-KO cells, we used the ATM kinase inhibitor (KU 55933). Inhibition of ATM signaling did not affect p53 activity in TIRR-KO cells (Figure S1E).

TIRR binds and regulates 53BP1 activity; therefore, the impact of TIRR on p53 may be mediated by 53BP1. Furthermore, a 53BP1-USP28 complex was identified as an activator of p53-mediated transactivation (Cuella-Martin et al., 2016; Fong et al., 2016; Lambrus et al., 2016; Meitinger et al., 2016). Therefore, we co-depleted either 53BP1 or USP28 in TIRR-KO cells and observed that the increased *p21* and *MDM2* expression in TIRR-KO cells was significantly suppressed upon the depletion of 53BP1 or USP28 proteins (Figures 1E, 1F, and S1F). We next used previously established binding null mutants of TIRR (K10E and R107S mutants) that do not interact with 53BP1 (Botuyan et al., 2018; Dai et al., 2018; Wang et al., 2018). We stably complemented the TIRR-KO cells with either wild-type (WT)-TIRR, or the binding null mutants of TIRR and examined p53-mediated gene transactivation. Consistent with our prior observations, the increase in *p21* and *MDM2* expression in TIRR-KO was rescued by WT TIRR but not by the K10E mutant (Figures 1G and 1H) or the R107S mutant (Figures S2A and S2B). These results indicate that TIRR loss causes aberrant p53-mediated transactivation in a 53BP1-dependent manner without inducing detectable DNA damage.

TIRR affects the promoter binding ability of p53 without impacting p53 stability or localization

To further investigate p53 activation in TIRR-depleted cells, we conducted quantitative image-based cytometry (QIBC) to quantify nuclear levels of p53 and its transcriptional target, p21, in individual cells. Stress-dependent induction of p21 nuclear intensity was increased primarily in G1 and G2 cells, consistent with previous work (Michelena et al., 2019; Sheng et al., 2019), with an at least 2-fold increase in TIRR-KO cells in all conditions (Figure 2A). In contrast to p21, no marked change in p53 nuclear intensity was observed (Figure 2B). Importantly, TIRR loss also did not significantly change the steady-state levels of p53 protein

Figure 1. TIRR loss increases 53BP1-dependent gene-transactivation property of p53

(A) Volcano plot showing differential gene expression in U2OS TIRR-KO cells. p values on the y axis were calculated using the DESeq2 algorithm (see Method details).

(B) Gene annotation and pathway analysis (core analysis of Ingenuity Pathway Analysis [IPA], QIAGEN) of the bulk RNA-sequencing (RNA-seq) data showing the top-ranked pathways that are significantly altered in TIRR-KO cells.

(C) qRT-PCR measurements from 3 independent experiments in RPE1 cells of indicated genotypes that were treated either with IR (5 Gy), Nutlin-3 (4 μM), or Centrinone (100 nM). Fold induction of *CDKN1A(p21)* and *MDM2* transcripts was normalized to *HPRT1* expression (means ± SDs) (*p = 0.0332–0.002; **p = 0.002–0.0002; ***p = 0.0002–0.0001; ****p < 0.0001; ns, p = 0.1234).

(D) Western blot in RPE1 cells of indicated genotype to confirm gene knockout.

(E) *p21* and *MDM2* transcript abundance measured by qRT-PCR in RPE1 WT and TIRR-KO cells that were transfected with indicated siRNAs and treated with Nutlin-3 for 4 h (means ± SDs) (*p = 0.0332–0.002; **p = 0.002–0.0002; ***p = 0.0002–0.0001; ****p < 0.0001; ns, p = 0.1234).

(F) p21 and MDM2 protein levels measured by immunoblot corresponding to (E).

(G) *p21* and *MDM2* transcript abundance measured by qRT-PCR in RPE1 TIRR-KO cells that stably expressed either WT or K10E mutant TIRR or an empty vector control through lentivirus-mediated transduction (means ± SDs) (*p = 0.0332–0.002; **p = 0.002–0.0002; ***p = 0.0002–0.0001; ****p < 0.0001; ns, p = 0.1234).

(H) p21 and MDM2 protein levels measured by immunoblot corresponding to (G).

Please cite this article in press as: Parnandi et al., TIRR inhibits the 53BP1-p53 complex to alter cell-fate programs, Molecular Cell (2021), https://doi.org/10.1016/j.molcel.2021.03.039

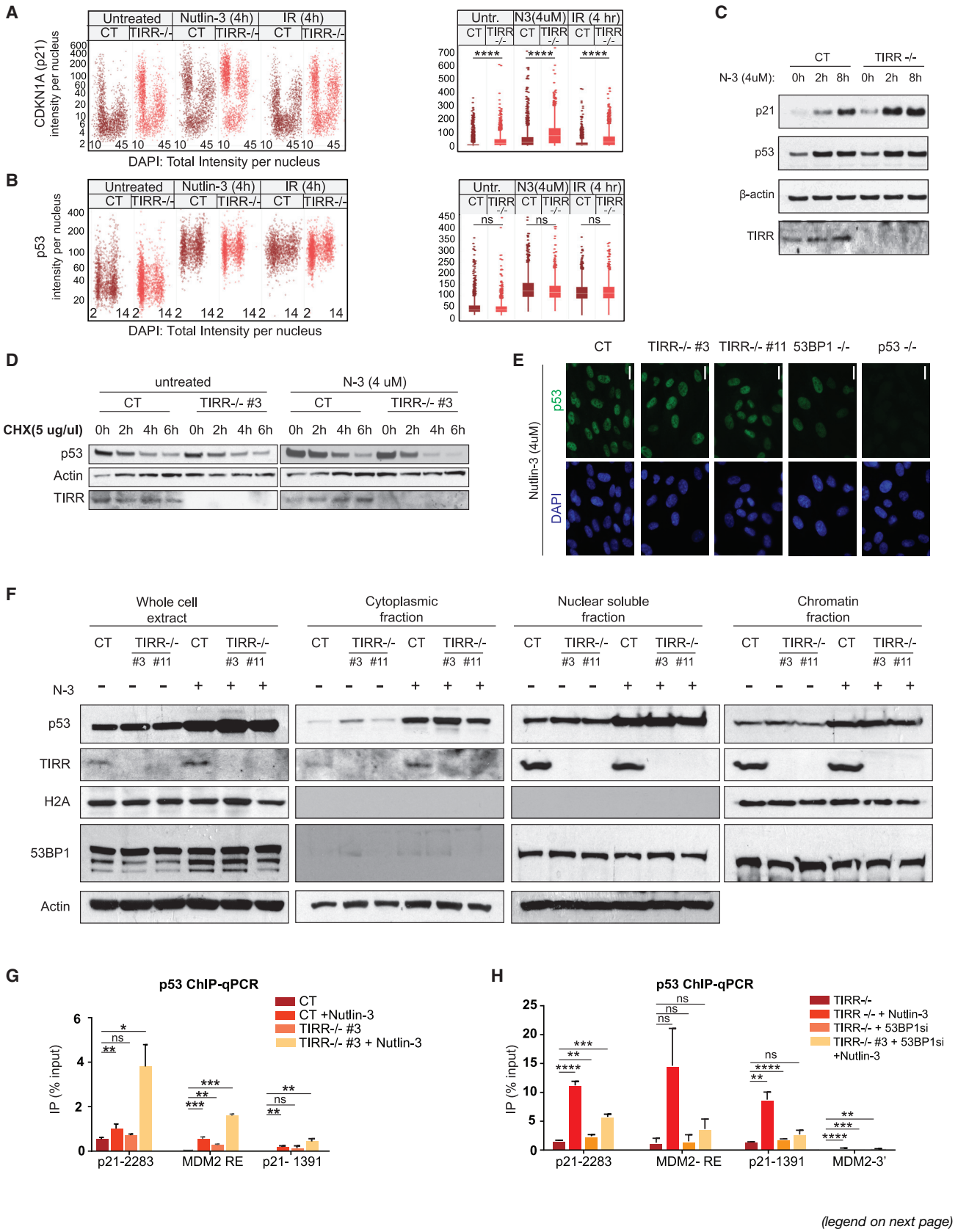

(legend on next page)

Please cite this article in press as: Parnandi et al., TIRR inhibits the 53BP1-p53 complex to alter cell-fate programs, Molecular Cell (2021), https://doi.org/10.1016/j.molcel.2021.03.039

(Figure 2C). Loss of TIRR did not affect the synthesis or degradation of p53 protein (Figures 2D and S2C). We also found no significant changes in p53 localization upon TIRR loss by immunofluorescence (Figure 2E) or biochemically in different subcellular fractions (Figure 2F). p53-mediated transactivation can be modulated by the stability, localization, or promoter binding efficiency of p53 protein (Lavin and Gueven, 2006). Since there were no significant changes in p53 protein stability or localization, we examined p53 occupancy at promoter-responsive elements (REs) by chromatin immunoprecipitation (ChIP) and qPCR in WT and TIRR-KO cells. Loss of TIRR increased p53 occupancy at the promoter RE site in *p21* by 4-fold and *MDM2* by 1.5-fold after Nutlin-3 treatment (Figure 2G). Depleting 53BP1 suppresses the higher p53 occupancy at promoter sites observed in TIRR-KO cells (Figure 2H). These results suggest that TIRR deficiency enhances p53 promoter binding efficiency but does not affect p53 stability or localization.

TIRR alters p53-mediated cell-fate programs by inhibiting the 53BP1-p53 interaction

p53 induces *CDKN1A(p21)* to promote cell-cycle arrest, *BAX* and BBC3/*PUMA* to initiate apoptosis, and *CDKN2A (p16^{Ink4a})* to induce cellular senescence (Mello and Attardi, 2018). Since we observed a significant upregulation of these target transcripts in TIRR-KO cells, we asked whether this translated to a change in overall cell-fate outcomes. To this end, we tested the effect of p53 activation by Nutlin-3 on cell survival in TIRR-KO cells. As anticipated, there was a ~40% reduction in cell survival due to Nutlin-3-induced growth arrest in TIRR-KO cells relative to control and a 200% increase in p53-KO cells (Figures 3A and 3B). We used resazurin cell viability assay as an alternative method to further validate these results and determined that TIRR loss significantly reduced survival in the presence of Nutlin-3 (half-maximal inhibitory concentration [IC_{50}] values of control (CT): 1.72 μM; TIRR$^{-/-}$ #3 : 1.034 μM; TIRR$^{-/-}$ #11 : 1.11 μM) (Figure 3C). The impact of TIRR loss on cell survival was rescued by WT TIRR but not by K10E TIRR, again indicating that the effect of TIRR on p53 function was mediated by its interaction with 53BP1 (Figure 3D). Next, we measured basal cellular senescence by β-galactosidase staining, and measured IR-induced expression of senescence-associated genes (*ANKRD1*, *EDN1*, and *IL6*) (Noren Hooten and Evans, 2017) . Consistent with our previous observations, there was a significant increase in the percentage of basal senescent cells in the absence of TIRR (Figure 3E) and an at least 2-fold increase in the expression of the senescence-associated genes in TIRR-KO cells after IR (Figure 3F). Finally, we tested the impact of TIRR on cell-cycle arrest and observed that there was a >5-fold decrease in the number of TIRR-KO cells in the S phase relative to WT cells after treatment with low doses of Nutlin-3 (Figures 3G and S2D). We also confirmed that this increase in p53 activity was not the result of accumulated endogenous damage due to the longer treatments with Nutlin-3 (Figure S2E).

These results establish that increased p53 activity caused by the loss of TIRR results in a significant change in p53-mediated cell-fate programs.

TIRR loss enhances the interaction of 53BP1 with p53

Previously, we had demonstrated that TIRR loss results in an "altered" form of 53BP1, which has increased binding capacity for its DNA repair effectors RIF1 and PTIP (Drané et al., 2017). A mutant 53BP1(F1553R) that does not interact with TIRR also mimics this altered activity (Botuyan et al., 2018). Based on these findings, we hypothesized that TIRR loss may affect the interaction of 53BP1 and p53. In TIRR-KO cells, we observed a striking 3-fold increase in endogenous 53BP1-p53 interaction by proximity ligation assay (PLA) after Nutlin-3 treatment (Figure 3H) or after exposure to IR and UV (Figure S2F). The increased 53BP1-p53 interaction in the absence of TIRR can be rescued by WT TIRR but not by K10E TIRR (Figure 3I). To further investigate the dynamics of the TIRR/53BP1/p53 associations, we used 3 probes in the PLA to visualize and quantify the 53BP1/p53 complex and the 53BP1/TIRR complex. We observed that these 2 complexes are distinct from each other and do not co-localize (Figure 3J). As a control, we either depleted 53BP1, which prevents the visualization of both complexes, or depleted p53, which specifically prevents tagging the 53BP1/p53 complex. To complement this cytological single-cell-based approach, we used a biochemical strategy using TIRR-KO cells. GFP-tagged p53 was transiently transfected in these cells that stably expressed FLAG-TIRR. The first step was FLAG immunoprecipitation to detect TIRR-interacting proteins. 53BP1 was found to be in the TIRR-bound fraction but endogenous and GFP-tagged p53 were both not found in this fraction. Next, the unbound fraction was used to immunoprecipitate GFP-p53-bound proteins. Here again, 53BP1 was identified as a p53-interacting partner but FLAG-TIRR was not (Figures 3K and 3L). We further confirmed that TIRR interacted with 53BP1 after p53

Figure 2. TIRR affects the promoter binding ability of p53, but has no effect on p53 protein turnover, stability, or localization

(A and B) WT and TIRR-KO U2OS cells were treated with different conditions (IR, Nutlin-3) for indicated time periods, and stained for p21 (A) or p53 (B) and DNA content, for cell-cycle-resolved quantification of nuclear levels of p21 and p53 by QIBC. Boxplots to the right show the quantification of nuclear protein intensities by QIBC analysis (means ± SDs) (*p = 0.0332–0.002; **p = 0.002–0.0002; ***p = 0.0002–0.0001; ****p < 0.0001; ns, p = 0.1234).

(C) p21 and p53 protein levels in RPE1 WT and TIRR-KO cells treated with Nutlin-3 at indicated time points. Actin was used as a loading control.

(D) p53 protein levels at different time points after treatment with 5 μg/μL cycloheximide in RPE1 CT and TIRR-KO cells.

(E) Immunofluorescence to show p53 localization in RPE1 cells of indicated genotype (scale bar, 20 μM).

(F) Western blot showing p53 proteins levels in different cellular fractions of RPE1 cells of indicated genotype that were either untreated or treated with Nutlin-3. Cells were first lysed in a hypotonic lysis buffer to extract the cytoplasmic fraction. The nuclear soluble fraction was extracted using a sucrose buffer and 350 mM NaCl, and the chromatin fraction was extracted using sucrose buffer containing 10% SDS. Actin was used as a loading control for the whole-cell extract, cytoplasmic, and nuclear soluble fractions, and H2A was used as a loading control for the chromatin fraction.

(G and H) ChIP-qPCR results measuring p53 occupancy at unique sites in *p21* and *MDM2* promoter regions. The data shown are representative of 2 experimental replicates. The bar plots indicate the ratio of immunoprecipitated DNA calculated relative to % total input, error bars indicate standard error (*p = 0.0332–0.002; **p = 0.002–0.0002; ***p = 0.0002–0.0001; ****p < 0.0001; ns, p = 0.1234).

Please cite this article in press as: Parnandi et al., TIRR inhibits the 53BP1-p53 complex to alter cell-fate programs, Molecular Cell (2021), https://doi.org/10.1016/j.molcel.2021.03.039

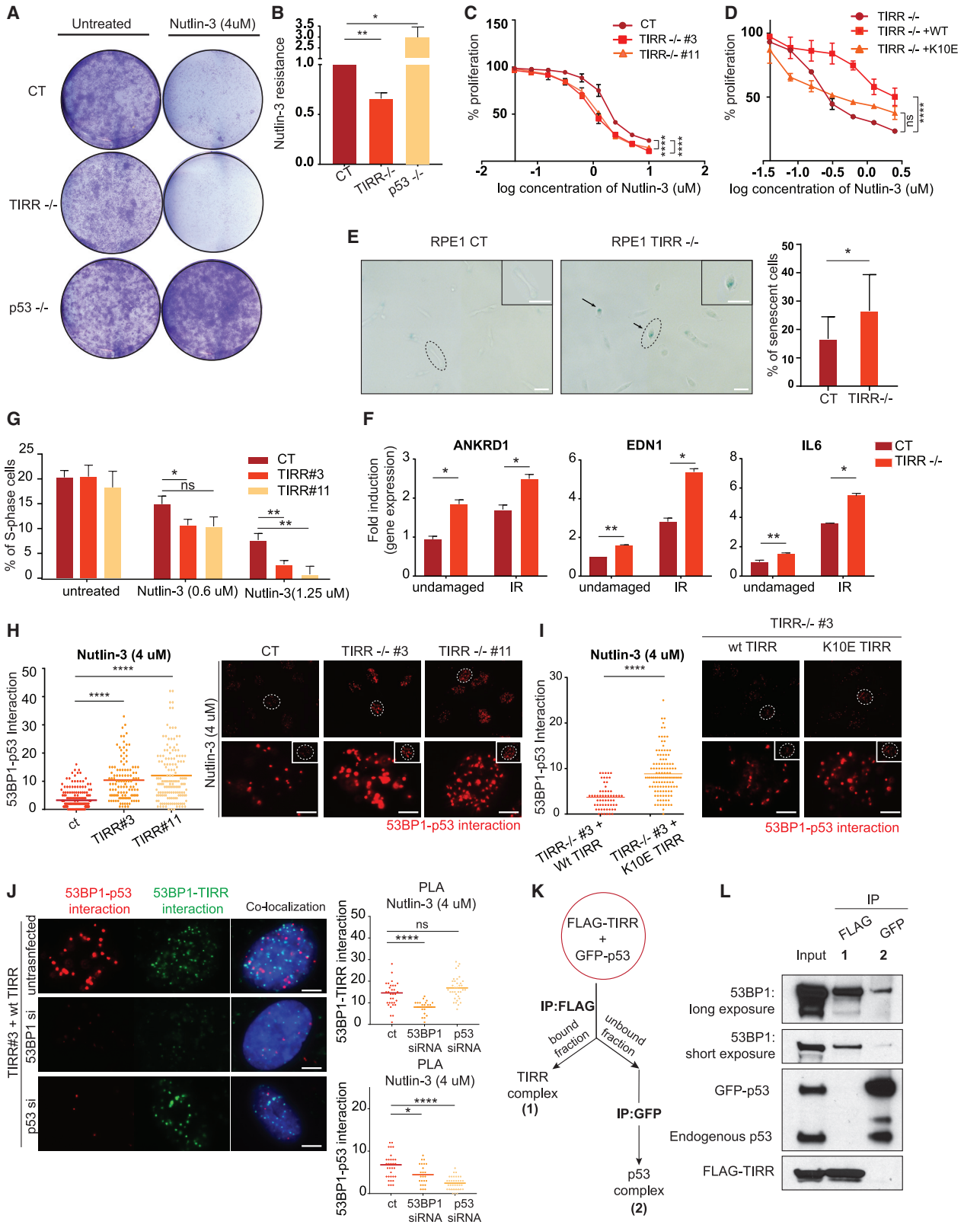

(legend on next page)

Please cite this article in press as: Parnandi et al., TIRR inhibits the 53BP1-p53 complex to alter cell-fate programs, Molecular Cell (2021), https://doi.org/10.1016/j.molcel.2021.03.039

activation, but there was no detectable interaction between TIRR and p53 (Figure S2G). These results strongly suggest that p53 is excluded from a 53BP1-TIRR complex and that TIRR is likely to impede the association of 53BP1 with p53.

TIRR inhibits the interaction of methylated p53 with the Tudor domain of 53BP1

To further understand the mechanism by which TIRR inhibits the 53BP1-p53 interaction, we considered the structural basis of the interactions of both TIRR and p53 proteins with 53BP1. Cell-based studies have suggested that the BRCT domain of 53BP1 is indispensable in regulating p53 activity (Cuella-Martin et al., 2016). However, structural studies suggest that the Tudor domain of 53BP1 interacts with p53 with an affinity comparable to that of the BRCT domain (Roy et al., 2010; Tong et al., 2015; Ekblad et al., 2004). The Tudor domain specifically interacts with dimethylated p53 (p53K370me2, p53K382me2). These modifications are associated with the gene transactivation functions of p53 (Huang et al., 2007; Kachirskaia et al., 2008; Tong et al., 2015). Therefore, we speculated that TIRR directly competes with dimethylated p53 for binding the Tudor domain, thereby negating the positive impact of the Tudor domain on the transactivation function of p53. To test this possibility, we used NMR spectroscopy to probe the interactions of 53BP1 alone and the 53BP1-TIRR complex with the C-terminal domain (CTD) region of p53 harboring a ^{13}C-labeled dimethyl lysine mimic at K370 (p53K_C370me2), or K382 (p53K_C382me2), or at both sites (p53K_C370me2K_C382me2). By monitoring the decrease in ^{1}H-^{13}C signal intensity associated with complex formation, we could demonstrate that TIRR impairs the interaction of 53BP1-Tudor with p53K_C370me2, p53K_C382me2, and p53K_C370me2K_C382me2 (Figures S3A and S3B). Furthermore, we tested whether purified WT TIRR can compete with p53 for the Tudor domain of 53BP1 in a similar NMR-based competition assay. We had previously established that the R107S mutant (Figures S2A and S2B) of TIRR does not bind the 53BP1 Tudor domain *in vitro* and in cells (Botuyan et al., 2018). Here, we observed that WT TIRR, but not the R107S binding null mutant, can displace p53K_C382me2 from the Tudor domain of 53BP1 (Figure 4A). Ubiquitin was used as a positive control in this assay (Figure S3C). We selected this K382 residue over K370 for our experiments because p53 dimethylated at K382 (p53K382me2) has significantly higher affinity for the Tudor domain than p53 dimethylated at K370 (p53K370me2), with respective K_d of 8 μM and 52 μM determined by isothermal titration calorimetry (ITC) (Figure 4B).

The site-specific DNA binding ability of p53 is attributed to both core DNA-binding domain (DBD) and the CTD domain of p53. In a previous cell-based analysis of 600 p53 RE sites, the WT p53 is bound to 355 sites, whereas the CTD mutant is bound to 210 of these sites, suggesting that both the DBD and CTD are important but not sufficient for the transcription factor (TF) activity of p53 (Laptenko et al., 2015; Sullivan et al., 2018). The DBD and CTD domains of p53 interact with distinct regions of 53BP1. The DBD interacts with the 53BP1-BRCT domain, whereas the CTD interacts with the 53BP1-Tudor domain. We asked whether TIRR regulates p53 activity by specifically blocking the p53-CTD and 53BP1-Tudor interaction. Endogenous p53 was transiently replaced with a CTD-deletion mutant or with a K382R mutant (Figure S4A). We observed that consistent with our previous results, *p21* and *MDM2* transcripts were induced in the TIRR-KO cells harboring WT-p53. However, this TIRR loss-mediated induction of p53 targets was completely suppressed by both CTD deletion and the K382R mutation of p53 (Figures 4C, 4D, and S4A). We also showed that the increased interaction of p53 and 53BP1 observed in TIRR KO cells is dependent on the CTD of p53 (Figure S4B). Based on these results, we inferred that the impact of TIRR on p53 activity is via its direct competition for the Tudor domain and is independent of the BRCT domain. To further validate this inference, we

Figure 3. TIRR alters p53-mediated cell-fate programs by inhibiting the p53-53BP1 interaction

(A and B) Sensitivity to Nutlin-3 measured by Crystal Violet staining. Representative images (A) and quantification of data (B) in RPE1 cells of indicated genotype. The experiment was performed in triplicate.

(C and D) Resazurin-based cell survival assay of RPE1 cells of indicated genotype treated with indicated concentrations of Nutlin-3 for 4 days. Experiments were performed in 3 replicates (****$p < 0.0001$; ns, $p > 0.05$).

(E) Representative images of senescent cells in RPE1 WT and TIRR-KO genetic backgrounds. Cells were fixed and stained for β-galactosidase as a senescence marker (scale bar, 100 μM). Bar plot represents the quantification of senescent cells (β-galactosidase$^+$) from 3 different replicates (*$p = 0.0332–0.002$; **$p = 0.002–0.0002$; ***$p = 0.0002–0.0001$; ****$p < 0.0001$; ns, $p = 0.1234$). (Lighter background on one half of the images was an artifact generated due to the positioning of the apotome).

(F) RPE1 WT and TIRR-KO cells were treated with IR (5 Gy) and recovered for 10 days. mRNA transcript levels of 3 senescence biomarkers, ANKRD1, EDN1, and IL-6, normalized to actin (means ± SDs) (*$p = 0.0332–0.002$; **$p = 0.002–0.0002$; ***$p = 0.0002–0.0001$; ****$p < 0.0001$; ns, $p = 0.1234$).

(G) RPE1 cells of indicated genotype were treated with Nutlin-3 for 72 h. The cells were fixed and stained for propidium iodide (PI). The data represent the number of cells in S phase from 3 different experiments measured by fluorescence-activated cell sorting (FACS) analysis using ModFit software (see Method details) (means ± SDs) (*$p = 0.0332–0.002$; **$p = 0.002–0.0002$; ***$p = 0.0002–0.0001$; ****$p < 0.0001$; ns, $p = 0.1234$).

(H and I) Representative images and quantification of endogenous 53BP1-p53 interaction in RPE1 cells of indicated genotype treated with Nutlin-3 using the proximity ligation assay (PLA; see Method details). Positive signals are indicated as red dots (scale bar, 5 μM).

(J) A 3-probe PLA assay assessing co-localization of TIRR-53BP1 and p53-53BP1 complexes in RPE1 TIRR-KO cells stably expressing WT TIRR (FLAG-WT TIRR). Cells were transfected with indicated siRNAs. The TIRR-p53 complex interaction is indicated by the green dots, and the p53-53BP1 complex interaction is indicated by the red dots (scale bar, 5 μM).

(K) Schematic of immunoprecipitation shown in (L). GFP-p53 was transfected in RPE1 TIRR-KO cells that were stably transduced by FLAG-tagged WT TIRR. FLAG-TIRR was immunoprecipitated to identify TIRR-interacting proteins. The fraction that was unbound to FLAG was used to immunoprecipitate GFP-p53 to identify p53-interacting proteins.

(L) Immunoblot of indicated proteins in 2 different interacting complexes (schematic in K). Complex 1 shows the interaction of FLAG-TIRR and 53BP1. Complex 2 shows the interaction of GFP-p53 and 53BP1.

Please cite this article in press as: Parnandi et al., TIRR inhibits the 53BP1-p53 complex to alter cell-fate programs, Molecular Cell (2021), https://doi.org/10.1016/j.molcel.2021.03.039

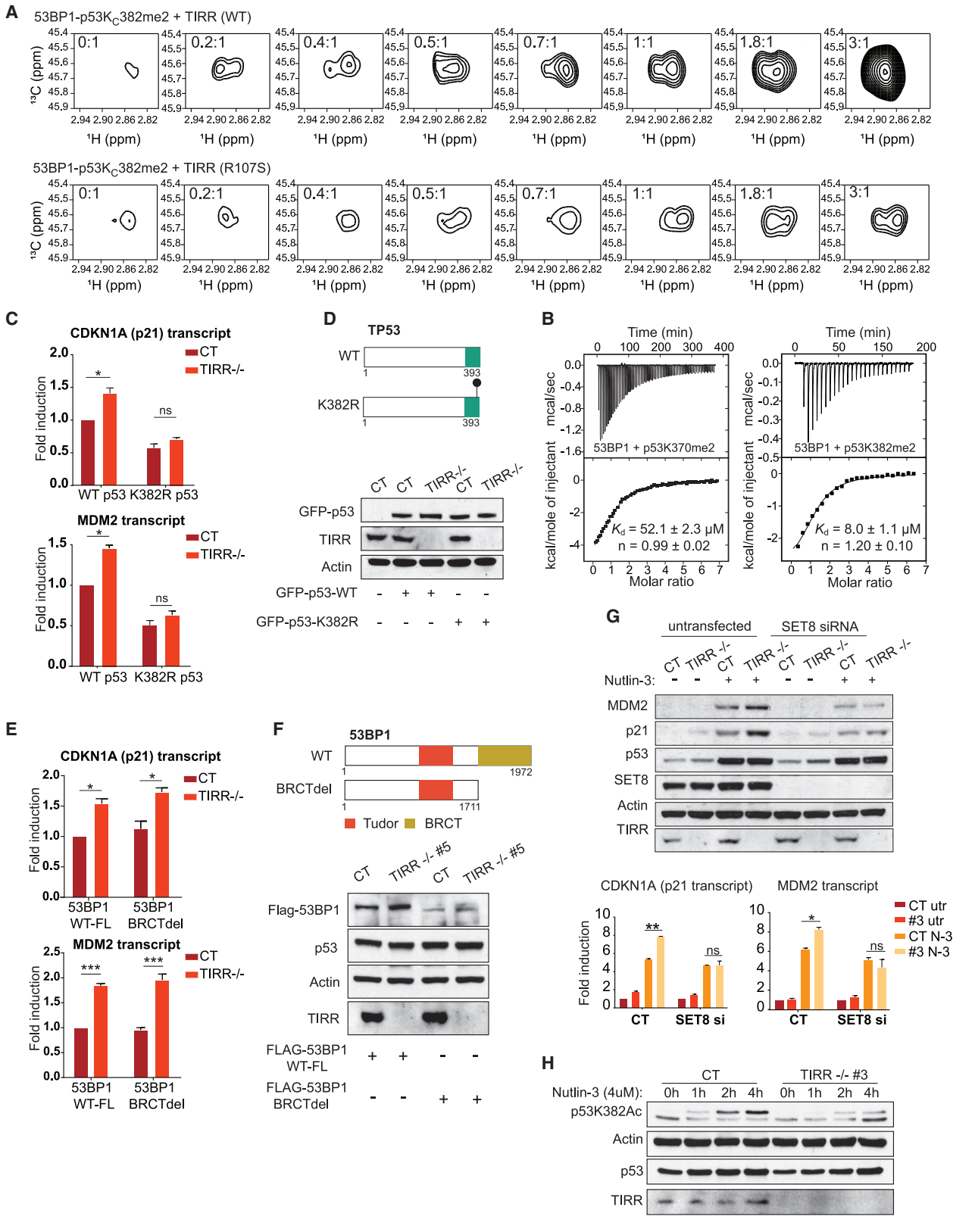

(legend on next page)

Please cite this article in press as: Parnandi et al., TIRR inhibits the 53BP1-p53 complex to alter cell-fate programs, Molecular Cell (2021), https://doi.org/10.1016/j.molcel.2021.03.039

expressed either the full-length 53BP1 or a BRCT-truncated form of 53BP1 in both WT and TIRR-KO cells and assessed the expression of *p21* and *MDM2* as a readout of p53 activity. We observed that the enhanced expression of *p21* and *MDM2* observed in TIRR-KO cells occurs independently of the BRCT domain of 53BP1 (Figures 4E and 4F).

Based on these findings, we hypothesized that in TIRR-KO cells there is increased availability of an uninhibited 53BP1-Tudor domain that binds dimethylated p53 (p53K382me2). This would suggest that the methylation of K382 is key to the phenotype induced by TIRR loss. To test this idea, we inhibited SET8, the monomethyl transferase that methylates p53 specifically at the residue K382 (Shi et al., 2007). The induction of p53 target transcripts that was observed in TIRR-KO cells was significantly suppressed by the inhibition of SET8 (Figure 4G). Previously it was shown that the methylation of certain key residues in the CTD of p53 (K370, K382) prevents another post-translational modification (PTM), acetylation, at the same residues (Shi et al., 2007; Kurash et al., 2008). Consistently, there was decreased acetylated p53 at residue K382 (p53K382ac) at different time points after Nutlin-3 treatment in TIRR-KO cells (Figure 4H). These results strongly support our model (Figure 5A) that TIRR inhibits p53-mediated transactivation by directly inhibiting the association of the CTD (primarily dimethylated at K382) of p53 with the 53BP1-Tudor domain.

TIRR negatively regulates p53 signaling in cancer

Our *in vitro* and cell line data thus far provide conclusive evidence that TIRR is a negative regulator of p53 transactivation. The tumor suppressor gene *TP53* is one of the most commonly altered genes in cancer, with loss-of-function mutations in >40% of all tumors. In ~6% of the remaining cancers, p53 signaling is altered by the amplification of the negative regulators MDM2 or MDM4 (Zehir et al., 2017). To assess whether the mutational profile of TIRR resembles that of other p53 regulators, we compared the frequency of genetic alterations present in *TIRR* with *MDM2* and *MDM4* (Figure 5B). We focused our analysis on The Cancer Genome Atlas (TCGA) invasive breast carcinoma and prostate adenocarcinoma cohorts, as these tumor types exhibit among the highest frequencies of *TIRR* amplification. Mutation and copy-number data revealed that *TIRR* amplifications are enriched in cancers that are *TP53* WT and lack *MDM2* or *MDM4* amplifications ($p = 0.015$ one-tailed Fisher's exact test), suggesting that *TIRR* amplifications are an alternative mechanism for the suppression of p53 activity. Next, we compared the expression of p53 pathway members in tumors that were classified as high or low TIRR, according to TIRR mRNA expression levels (using a *Z* score cutoff of 3). We used the average expression of 15 downstream targets of p53, including negative feedback regulators and genes involved in DNA repair, cell-cycle arrest, apoptosis, and metastasis inhibition (Figure 5C). As anticipated, both breast and prostate tumors with high TIRR expression showed decreased levels of p53 pathway expression (Figure 5C; $p = 0.0098$ and $p = 0.0019$, Wilcoxon test). This was comparable to the correlation of *MDM2*/*MDM4* amplification and the expression of the same set of p53 target genes in breast and prostate carcinomas, indicating that TIRR acts as a negative regulator of p53 (Figure S4C). The loss of TIRR amplifies the function of p53, which would be detrimental for tumorigenesis. Therefore, we predicted that p53-proficient tumors are likely to have stable TIRR expression or may enhance TIRR expression to suppress p53. This would be in contrast to p53-deficient tumors, which would not have selective pressure to retain TIRR expression. To test this prediction, we analyzed and contrasted TIRR mRNA expression between renal clear cell carcinomas, <4% of which exhibit *TP53* mutations, and serous ovarian cancers, in which *TP53* mutation frequencies are >80% (Figure 5D). While ovarian cancers frequently exhibit copy loss of TIRR, renal cancers do not. Moreover, TIRR expression changes markedly with copy number in ovarian cancers but not renal cancers. These findings suggest that renal cancers, with intact TP53, do not tolerate changes, especially losses in

Figure 4. TIRR inhibits the interaction of methylated p53 with the Tudor domain of 53BP1

(A) Changes in the ^{1}H-^{13}C correlation methyl NMR signals of the preformed 53BP1-Tudor-p53K_C382me2 complex harboring ^{13}C-labeled K_C382me2 methyl groups upon titration with WT TIRR and binding null mutant TIRR (R107S). The ratios of WT TIRR and R107S TIRR with respect to 53BP1-Tudor-p53K_C382me2 are indicated. The increase in signal intensity with increased concentration of TIRR indicates that, as expected, WT TIRR displaces p53K_C382me2 from 53BP1.

(B) 53BP1-Tudor was titrated with p53K370me2 (366-375) and p53K382me2 (377–386) peptides. For each titration, the raw data and integrated heat measurements with curve fitting using a 1-site binding model are indicated. The K_ds and stoichiometry numbers n are indicated with associated SDs determined by nonlinear least-squares analysis.

(C) *p21* and *MDM2* transcript levels calculated by qRT-PCR in RPE1 cells of indicated genotype. The cells were treated with p53 siRNA to deplete endogenous p53 and transiently transfected with siRNA-resistant constructs expressing either WT p53 or the K382R mutant; (means ± SDs) (*p = 0.0332–0.002; **p = 0.002–0.0002; ***p = 0.0002–0.0001; ****p < 0.0001; ns, p = 0.1234).

(D) Schematic representation of the p53 constructs used in (C); immunoblots comparing expression levels of the 2 p53 constructs used in (C) in cells of the indicated genotype.

(E) *p21* and *MDM2* transcript levels calculated by qRT-PCR in U2OS cells of indicated genotype. Cells were treated with a 3′ UTR siRNA to deplete endogenous 53BP1 and transiently transfected with either a full-length 53BP1 or a truncated mutant lacking the BRCT domain; (means ± SDs) (*p = 0.0332–0.002; **p = 0.002–0.0002; ***p = 0.0002–0.0001; ****p < 0.0001; ns, p = 0.1234).

(F) Schematic representation of 53BP1 constructs used in (E); immunoblots comparing expression levels of the 2 53BP1 constructs used in (E) in cells of the indicated genotype.

(G) RPE1 cells of indicated genotype were transfected with an siRNA against SET8; 48 h after transfection, the cells were either untreated or treated with Nutlin-3. The western blot indicates p21 and MDM2 protein levels in the indicated genotypes and treatments. The corresponding *p21* and *MDM2* transcript abundance calculated by qRT-PCR is represented in the bar graphs; (means ± SDs) (*p = 0.0332–0.002; **p = 0.002–0.0002; ***p = 0.0002–0.0001; ****p < 0.0001; ns, p = 0.1234).

(H) Western blot depicts the levels of indicated proteins. RPE1 CT and TIRR-KO cells, either untreated or treated with Nutlin-3, were extracted at different time points to examine the levels of acetylated p53 at residue K382 (p53K382ac).

Please cite this article in press as: Parnandi et al., TIRR inhibits the 53BP1-p53 complex to alter cell-fate programs, Molecular Cell (2021), https://doi.org/10.1016/j.molcel.2021.03.039

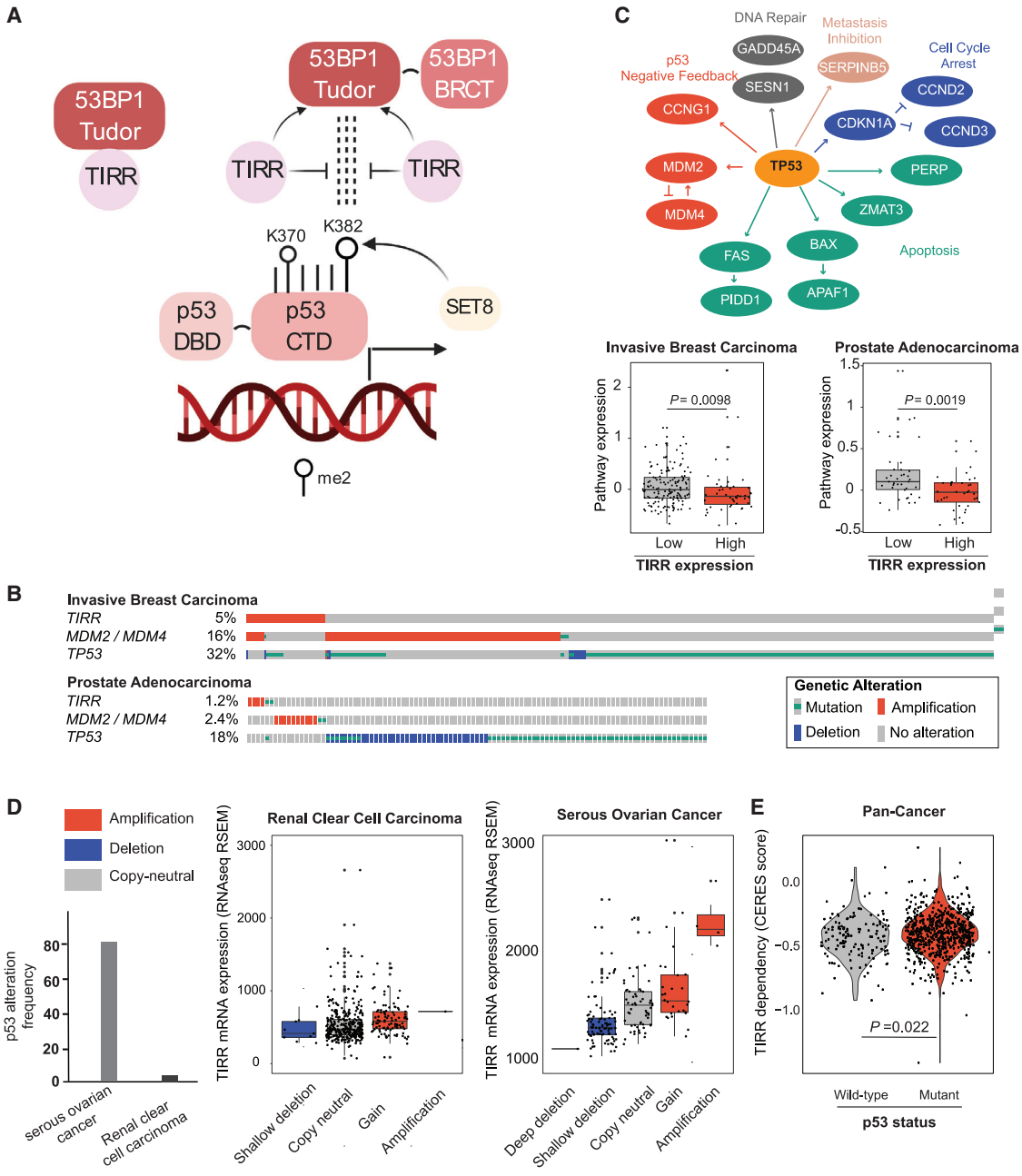

Figure 5. TIRR negatively regulates p53 signaling in cancer

(A) Model depicting TIRR as an upstream regulator of the 53BP1-p53 axis involved in p53 transactivation. The Tudor domain of 53BP1 interacts with p53K382me2, a PTM of p53 that is associated with the higher transactivation of p53. TIRR competes with dimethylated p53 for the Tudor domain of 53BP1.

(B) OncoPrint showing the frequency at which *TIRR*, *MDM2*/*MDM4,* and *TP53* are altered in invasive breast carcinoma and prostate adenocarcinoma cohorts from TCGA (The Cancer Genome Atlas Network, 2012; Hoadley et al., 2018). For visualization purposes, only samples with genetic alterations are shown in the plot. Putative driver mutations were chosen based on OncoKB driver annotations and copy-number alterations were selected on GISTIC calls. OncoPrints were generated in the cBioPortal for Cancer Genomics (www.cbioportal.org).

(C) Genes belonging to the p53 pathway for which expression data were used to calculate pathway expression estimates. Pathway expression in invasive breast carcinoma and prostate adenocarcinoma samples with and without TIRR amplification. Pathway expression scores were calculated as the average mRNA expression of p53 pathway members. RNA-seq data for each p53 pathway gene were obtained from TCGA and were evaluated as *Z* scores relative to diploid samples. p values, Wilcoxon test.

(D) The level at which loss of TIRR is tolerated in human cancers is dependent on p53 status. Cancers with high frequencies of p53 alterations (serous ovarian cancer, right) can tolerate changes in TIRR expression through genomic loss, as a compensating mechanism for p53 activity. However, cancers with low

(legend continued on next page)

Please cite this article in press as: Parnandi et al., TIRR inhibits the 53BP1-p53 complex to alter cell-fate programs, Molecular Cell (2021), https://doi.org/10.1016/j.molcel.2021.03.039

TIRR expression, whereas ovarian cancers that have lost TP53 are less reliant on TIRR. This is further supported by TIRR dependency analysis of 769 Cancer Cell Line Encyclopedia (CCLE) lines (136 of which are p53 WT and 633 are p53 mutant), which showed that p53-proficient lines were significantly more dependent on *TIRR* (Figure 5E). These analyses suggested that TIRR amplification may be an important mechanism by which cancers suppress p53 activity.

DISCUSSION

Over 25 years ago, 53BP1 was discovered as a p53-interacting protein (Iwabuchi et al., 1994). A decade later, animal model-based studies showed that the DNA repair function of 53BP1 and the role of p53 in checkpoint control and apoptosis synergized to prevent tumorigenesis (Morales et al., 2006; Ward et al., 2005). However, the link of 53BP1 to p53 faded over the years, as 53BP1 emerged as a central player in the repair of DSBs. More recently, 53BP1, USP28, and p53 were identified in 3 related screens aimed at identifying the suppressors of the cell-cycle arrest induced either by reducing the centriole number or by prolonged mitotic arrest (Fong et al., 2016; Lambrus et al., 2016; Meitinger et al., 2016). The mechanism proposed was that 53BP1 and USP28 promote p53 protein stability specifically in the context of mitotic stress, but not by DNA damage or by Nutlin-3. In contrast, Cuella-Martin et al. (2016) observed that the loss of 53BP1 did not affect p53 levels but significantly diminished p53 transactivation function after IR or Nutlin-3 treatment. Structural studies have shown that both the BRCT and Tudor domains of 53BP1 can directly interact with p53 (Derbyshire et al., 2002; Joo et al., 2002; Kachirskaia et al., 2008; Roy et al., 2010; Tong et al., 2015). More recently, however, the BRCT domain and the oligomerization domain of 53BP1 were implicated in the activation of p53 (Cuella-Martin et al., 2016; Kilic et al., 2019). Collectively, these studies have highlighted the importance of the 53BP1/p53 complex and raised several unanswered questions: (1) does 53BP1 regulate p53 function beyond mitotic stress? (2) what is the underlying molecular mechanism of 53BP1-mediated regulation of the function of p53? and (3) are there any molecular/biochemical links between the function of 53BP1 in DSB repair and p53 activation? Here, our results provide insight into these unresolved issues by elucidating the functional and biochemical interplay of TIRR, 53BP1, and p53 in cells and *in vitro*.

The site-specific DNA-binding ability of p53 is mediated by its core DBD and the CTD (Laptenko et al., 2015; Anderson et al., 1997; Laptenko and Prives, 2006; Luo et al., 2004; Bieging et al., 2014), and this in turn influences its transactivation function. p53 dimethylated at residues K370 and K382 in the CTD is poised for higher transactivation (DeHart et al., 2014; Huang et al., 2007; Kachirskaia et al., 2008), and these residues are also involved in direct interaction with the Tudor domain of 53BP1 (Kachirskaia et al., 2008; Roy et al., 2010; Tong et al., 2015). From our results we have inferred that TIRR downmodulates p53 activity by specifically inhibiting the Tudor-p53K382me2 interaction. The inhibition of p53 activity by TIRR is dependent on the Tudor domain of 53BP1 and independent of the BRCT domain. Prior work suggested that the role of USP28 in regulating p53 was downstream of 53BP1 and it was via the BRCT domain of 53BP1. However, it was not clear whether USP28 deubiquitinates p53 to stabilize it or regulates its DNA-binding function, or whether its impact on p53 is indirect, via other factors. Intriguingly, USP28 is also functionally involved in the TIRR-mediated regulation of p53 (Figure S1E). Future work will ascertain the precise role of USP28 in the TIRR/53BP1/p53 signaling network. Analysis of TCGA data revealed the striking similarity between MDM2/4, the established negative regulator of p53, and TIRR. Most intriguing, we observed cancers that had low p53 alteration frequency had maintained stable expression of TIRR with almost no loss or deletion of the TIRR gene. This is consistent with the notion that TIRR loss in these p53-proficient tumors would enhance p53 activity and impair tumor growth. In contrast, p53-deficient tumors have no such incentive to retain TIRR, which is evident by the significant number of tumors with deletions of the *TIRR* gene locus. Our results indicated that TIRR may represent a distinct and hitherto undiscovered mechanism for inactivating p53 in primary tumors. Further analysis of cancer databases is necessary to solidify this intriguing concept.

A comprehensive analysis of 44 datasets from human p53 ChIP-seq studies revealed that only 11% of all p53-bound sites near the transcription start site (TSS) of genes result in differential expression (Nguyen et al., 2018). The lack of correspondence between binding and expression suggests that additional context-dependent signals, including cofactors such as 53BP1, are required for an efficient p53 transcriptional response. A limitation of this study is that we have not addressed which p53 target transcripts are regulated directly by 53BP1/TIRR. Furthermore, TIRR may affect p53 function beyond its regulation of 53BP1. These two issues should be addressed in future work.

STAR★METHODS

Detailed methods are provided in the online version of this paper and include the following:

- KEY RESOURCES TABLE
- RESOURCE AVAILABILITY
  - Lead contact
  - Materials availability
  - Data and code availability
- EXPERIMENTAL MODEL AND SUBJECT DETAILS
  - Gene editing
- METHOD DETAILS

frequencies of p53 alterations (renal cancer, left) do not tolerate changes in TIRR expression that cause changes in p53 activity. Copy-number events have been colored to indicate losses (blue) or gains (red) of genomic material. Gene expression (*Z* scores from RNA-seq V2 RSEM) and copy-number data were downloaded from TCGA (The Cancer Genome Atlas Network, 2012).

(E) Comparison of TIRR dependency scores (CERES) between 136 p53 WT and 633 p53 mutant cancer cell lines. p53 WT cell lines have a significantly higher dependency on *TIRR*. Dependency scores were calculated using DepMap's Achilles Avana 20Q2 public release (https://portals.broadinstitute.org/ccle).

- Retrovirus production
- RNAi
- RNA extraction and RT-PCR
- Immunoprecipitation and western blotting
- Proximity ligation assay
- Chromatin immunoprecipitation
- PI staining and FACS
- Senescence assay
- Cell survival assays
- Bioinformatics
- Preparation of proteins and peptides for NMR spectroscopy and ITC studies
- NMR spectroscopy
- Isothermal titration calorimetry
- QIBC
- RNA-seq differential gene expression analysis and pathway analysis

- QUANTIFICATION AND STATISTICAL ANALYSIS

SUPPLEMENTAL INFORMATION

Supplemental information can be found online at https://doi.org/10.1016/j.molcel.2021.03.039.

ACKNOWLEDGMENTS

D.C. is supported by R01 CA208244, Gray Foundation Team Science Award, DOD Ovarian Cancer Award W81XWH-15-0564/OC140632, Tina's Wish Foundation, and the Claudia Adams Barr Program in Innovative Basic Cancer Research. G.M. is supported by NIH grants R01 CA132878 and R35 GM136262. M.V.B. acknowledges support from an OCRA Liz Tilberis Award. M.A. is supported by the Swiss National Science Foundation (PP00P3_179057 and 310030_197003) and by the European Research Council (ERC) under the European Union's Horizon 2020 research and innovation program (ERC-2016-STG 714326). We thank Sharmistha Pal for sharing protocols and reagents and Shrabasti Roychoudhury for comments on the manuscript.

AUTHOR CONTRIBUTIONS

N.P. and D.C. conceived the study and wrote the paper, with input from V.R., M.V.B., H.N., M.A., G.M., and R.B. The RNA-seq data were acquired by P.D., and analyzed by H.N. The QIBC experiments were conducted and analyzed by M.R., under the supervision of M.A. The NMR and ITC experiments were conducted by G.C., and the protein purification for the same was carried out by M.V.B., under the supervision of G.M. The bioinformatic analysis was done by V.R., under the supervision of R.B. All of the other experiments were carried out by N.P., under the supervision of D.C.

DECLARATION OF INTERESTS

D.C. is a member of the Advisory Board of *Molecular Cell*.

Received: September 2, 2020
Revised: January 19, 2021
Accepted: March 24, 2021
Published: May 6, 2021

REFERENCES

Anderson, M.E., Woelker, B., Reed, M., Wang, P., and Tegtmeyer, P. (1997). Reciprocal interference between the sequence-specific core and nonspecific C-terminal DNA binding domains of p53: implications for regulation. Mol. Cell. Biol. *17*, 6255–6264.

Benirschke, R.C., Thompson, J.R., Nominé, Y., Wasielewski, E., Juranić, N., Macura, S., Hatakeyama, S., Nakayama, K.I., Botuyan, M.V., and Mer, G. (2010). Molecular basis for the association of human E4B U box ubiquitin ligase with E2-conjugating enzymes UbcH5c and Ubc4. Structure *18*, 955–965.

Bieging, K.T., Mello, S.S., and Attardi, L.D. (2014). Unravelling mechanisms of p53-mediated tumour suppression. Nat. Rev. Cancer *14*, 359–370.

Botuyan, M.V., Lee, J., Ward, I.M., Kim, J.E., Thompson, J.R., Chen, J., and Mer, G. (2006). Structural basis for the methylation state-specific recognition of histone H4-K20 by 53BP1 and Crb2 in DNA repair. Cell *127*, 1361–1373.

Botuyan, M.V., Cui, G., Drané, P., Oliveira, C., Detappe, A., Brault, M.E., Parnandi, N., Chaubey, S., Thompson, J.R., Bragantini, B., et al. (2018). Mechanism of 53BP1 activity regulation by RNA-binding TIRR and a designer protein. Nat. Struct. Mol. Biol. *25*, 591–600.

Chapman, J.R., Taylor, M.R., and Boulton, S.J. (2012). Playing the end game: DNA double-strand break repair pathway choice. Mol. Cell *47*, 497–510.

Cuella-Martin, R., Oliveira, C., Lockstone, H.E., Snellenberg, S., Grolmusova, N., and Chapman, J.R. (2016). 53BP1 Integrates DNA Repair and p53-Dependent Cell Fate Decisions via Distinct Mechanisms. Mol. Cell *64*, 51–64.

Cui, G., Botuyan, M.V., and Mer, G. (2009). Preparation of recombinant peptides with site- and degree-specific lysine (13)C-methylation. Biochemistry *48*, 3798–3800.

Dai, Y., Zhang, A., Shan, S., Gong, Z., and Zhou, Z. (2018). Structural basis for recognition of 53BP1 tandem Tudor domain by TIRR. Nat. Commun. *9*, 2123.

DeHart, C.J., Chahal, J.S., Flint, S.J., and Perlman, D.H. (2014). Extensive post-translational modification of active and inactivated forms of endogenous p53. Mol. Cell. Proteomics *13*, 1–17.

Derbyshire, D.J., Basu, B.P., Serpell, L.C., Joo, W.S., Date, T., Iwabuchi, K., and Doherty, A.J. (2002). Crystal structure of human 53BP1 BRCT domains bound to p53 tumour suppressor. EMBO J. *21*, 3863–3872.

Drané, P., Brault, M.E., Cui, G., Meghani, K., Chaubey, S., Detappe, A., Parnandi, N., He, Y., Zheng, X.F., Botuyan, M.V., et al. (2017). TIRR regulates 53BP1 by masking its histone methyl-lysine binding function. Nature *543*, 211–216.

Durocher, D., and Pelletier, L. (2016). 53BP1 Goes Back to Its p53 Roots. Mol. Cell *64*, 3–4.

Ekblad, C.M., Friedler, A., Veprintsev, D., Weinberg, R.L., and Itzhaki, L.S. (2004). Comparison of BRCT domains of BRCA1 and 53BP1: a biophysical analysis. Protein Sci. *13*, 617–625.

Fong, C.S., Mazo, G., Das, T., Goodman, J., Kim, M., O'Rourke, B.P., Izquierdo, D., and Tsou, M.F. (2016). 53BP1 and USP28 mediate p53-dependent cell cycle arrest in response to centrosome loss and prolonged mitosis. eLife *5*, e16270.

Frankish, A., Diekhans, M., Ferreira, A.M., Johnson, R., Jungreis, I., Loveland, J., Mudge, J.M., Sisu, C., Wright, J., Armstrong, J., et al. (2019). GENCODE reference annotation for the human and mouse genomes. Nucleic Acids Res. *47* (D1), D766–D773.

Gingrich, T.R., Rotskoff, G.M., Crooks, G.E., and Geissler, P.L. (2016). Near-optimal protocols in complex nonequilibrium transformations. Proc. Natl. Acad. Sci. USA *113*, 10263–10268.

Hoadley, K.A., Yau, C., Hinoue, T., Wolf, D.M., Lazar, A.J., Drill, E., Shen, R., Taylor, A.M., Cherniack, A.D., Thorsson, V., et al.; The Cancer Genome Atlas Network (2018). Cell-of-Origin Patterns Dominate the Molecular Classification of 10,000 Tumors from 33 Types of Cancer. Cell *173*, 291–304.e6.

Huang, J., Sengupta, R., Espejo, A.B., Lee, M.G., Dorsey, J.A., Richter, M., Opravil, S., Shiekhattar, R., Bedford, M.T., Jenuwein, T., and Berger, S.L. (2007). p53 is regulated by the lysine demethylase LSD1. Nature *449*, 105–108.

Iwabuchi, K., Bartel, P.L., Li, B., Marraccino, R., and Fields, S. (1994). Two cellular proteins that bind to wild-type but not mutant p53. Proc. Natl. Acad. Sci. USA *91*, 6098–6102.

Johnson, B.A. (2018). From Raw Data to Protein Backbone Chemical Shifts Using NMRFx Processing and NMRViewJ Analysis. Methods Mol. Biol. *1688*, 257–310.

Joo, W.S., Jeffrey, P.D., Cantor, S.B., Finnin, M.S., Livingston, D.M., and Pavletich, N.P. (2002). Structure of the 53BP1 BRCT region bound to p53 and its comparison to the Brca1 BRCT structure. Genes Dev. *16*, 583–593.

Kachirskaia, I., Shi, X., Yamaguchi, H., Tanoue, K., Wen, H., Wang, E.W., Appella, E., and Gozani, O. (2008). Role for 53BP1 Tudor domain recognition of p53 dimethylated at lysine 382 in DNA damage signaling. J. Biol. Chem. *283*, 34660–34666.

Kilic, S., Lezaja, A., Gatti, M., Bianco, E., Michelena, J., Imhof, R., and Altmeyer, M. (2019). Phase separation of 53BP1 determines liquid-like behavior of DNA repair compartments. EMBO J. *38*, e101379.

Kurash, J.K., Lei, H., Shen, Q., Marston, W.L., Granda, B.W., Fan, H., Wall, D., Li, E., and Gaudet, F. (2008). Methylation of p53 by Set7/9 mediates p53 acetylation and activity in vivo. Mol. Cell *29*, 392–400.

Lambrus, B.G., Daggubati, V., Uetake, Y., Scott, P.M., Clutario, K.M., Sluder, G., and Holland, A.J. (2016). A USP28-53BP1-p53-p21 signaling axis arrests growth after centrosome loss or prolonged mitosis. J. Cell Biol. *214*, 143–153.

Laptenko, O., and Prives, C. (2006). Transcriptional regulation by p53: one protein, many possibilities. Cell Death Differ. *13*, 951–961.

Laptenko, O., Shiff, I., Freed-Pastor, W., Zupnick, A., Mattia, M., Freulich, E., Shamir, I., Kadouri, N., Kahan, T., Manfredi, J., et al. (2015). The p53 C terminus controls site-specific DNA binding and promotes structural changes within the central DNA binding domain. Mol. Cell *57*, 1034–1046.

Lavin, M.F., and Gueven, N. (2006). The complexity of p53 stabilization and activation. Cell Death Differ. *13*, 941–950.

Love, M.I., Huber, W., and Anders, S. (2014). Moderated estimation of fold change and dispersion for RNA-seq data with DESeq2. Genome Biol. *15*, 550.

Luo, J., Li, M., Tang, Y., Laszkowska, M., Roeder, R.G., and Gu, W. (2004). Acetylation of p53 augments its site-specific DNA binding both in vitro and in vivo. Proc. Natl. Acad. Sci. USA *101*, 2259–2264.

Meitinger, F., Anzola, J.V., Kaulich, M., Richardson, A., Stender, J.D., Benner, C., Glass, C.K., Dowdy, S.F., Desai, A., Shiau, A.K., and Oegema, K. (2016). 53BP1 and USP28 mediate p53 activation and G1 arrest after centrosome loss or extended mitotic duration. J. Cell Biol. *214*, 155–166.

Mello, S.S., and Attardi, L.D. (2018). Deciphering p53 signaling in tumor suppression. Curr. Opin. Cell Biol. *51*, 65–72.

Michelena, J., Gatti, M., Teloni, F., Imhof, R., and Altmeyer, M. (2019). Basal CHK1 activity safeguards its stability to maintain intrinsic S-phase checkpoint functions. J. Cell Biol. *218*, 2865–2875.

Morales, J.C., Franco, S., Murphy, M.M., Bassing, C.H., Mills, K.D., Adams, M.M., Walsh, N.C., Manis, J.P., Rassidakis, G.Z., Alt, F.W., and Carpenter, P.B. (2006). 53BP1 and p53 synergize to suppress genomic instability and lymphomagenesis. Proc. Natl. Acad. Sci. USA *103*, 3310–3315.

Nguyen, T.T., Grimm, S.A., Bushel, P.R., Li, J., Li, Y., Bennett, B.D., Lavender, C.A., Ward, J.M., Fargo, D.C., Anderson, C.W., et al. (2018). Revealing a human p53 universe. Nucleic Acids Res. *46*, 8153–8167.

Noren Hooten, N., and Evans, M.K. (2017). Techniques to Induce and Quantify Cellular Senescence. J. Vis. Exp. (123), 55533.

Robinson, M.D., McCarthy, D.J., and Smyth, G.K. (2010). edgeR: a Bioconductor package for differential expression analysis of digital gene expression data. Bioinformatics *26*, 139–140.

Roy, S., Musselman, C.A., Kachirskaia, I., Hayashi, R., Glass, K.C., Nix, J.C., Gozani, O., Appella, E., and Kutateladze, T.G. (2010). Structural insight into p53 recognition by the 53BP1 tandem Tudor domain. J. Mol. Biol. *398*, 489–496.

Sheng, C., Mendler, I.H., Rieke, S., Snyder, P., Jentsch, M., Friedrich, D., Drossel, B., and Loewer, A. (2019). PCNA-Mediated Degradation of p21 Coordinates the DNA Damage Response and Cell Cycle Regulation in Individual Cells. Cell Rep. *27*, 48–58.e7.

Shi, X., Kachirskaia, I., Yamaguchi, H., West, L.E., Wen, H., Wang, E.W., Dutta, S., Appella, E., and Gozani, O. (2007). Modulation of p53 function by SET8-mediated methylation at lysine 382. Mol. Cell *27*, 636–646.

Soneson, C., Love, M.I., and Robinson, M.D. (2015). Differential analyses for RNA-seq: transcript-level estimates improve gene-level inferences. F1000Res. *4*, 1521.

Sullivan, K.D., Galbraith, M.D., Andrysik, Z., and Espinosa, J.M. (2018). Mechanisms of transcriptional regulation by p53. Cell Death Differ. *25*, 133–143.

The Cancer Genome Atlas Network (2012). Comprehensive molecular portraits of human breast tumours. Nature *490*, 61–70.

Tong, Q., Cui, G., Botuyan, M.V., Rothbart, S.B., Hayashi, R., Musselman, C.A., Singh, N., Appella, E., Strahl, B.D., Mer, G., and Kutateladze, T.G. (2015). Structural plasticity of methyllysine recognition by the tandem tudor domain of 53BP1. Structure *23*, 312–321.

Wang, J., Yuan, Z., Cui, Y., Xie, R., Yang, G., Kassab, M.A., Wang, M., Ma, Y., Wu, C., Yu, X., and Liu, X. (2018). Molecular basis for the inhibition of the methyl-lysine binding function of 53BP1 by TIRR. Nat. Commun. *9*, 2689.

Ward, I.M., Difilippantonio, S., Minn, K., Mueller, M.D., Molina, J.R., Yu, X., Frisk, C.S., Ried, T., Nussenzweig, A., and Chen, J. (2005). 53BP1 cooperates with p53 and functions as a haploinsufficient tumor suppressor in mice. Mol. Cell. Biol. *25*, 10079–10086.

Zehir, A., Benayed, R., Shah, R.H., Syed, A., Middha, S., Kim, H.R., Srinivasan, P., Gao, J., Chakravarty, D., Devlin, S.M., et al. (2017). Mutational landscape of metastatic cancer revealed from prospective clinical sequencing of 10,000 patients. Nat. Med. *23*, 703–713.

Zhang, A., Peng, B., Huang, P., Chen, J., and Gong, Z. (2017). The p53-binding protein 1-Tudor-interacting repair regulator complex participates in the DNA damage response. J. Biol. Chem. *292*, 6461–6467.

Zimmermann, M., and de Lange, T. (2014). 53BP1: pro choice in DNA repair. Trends Cell Biol. *24*, 108–117.

Please cite this article in press as: Parnandi et al., TIRR inhibits the 53BP1-p53 complex to alter cell-fate programs, Molecular Cell (2021), https://doi.org/10.1016/j.molcel.2021.03.039

STAR★METHODS

KEY RESOURCES TABLE

REAGENT or RESOURCE	SOURCE	IDENTIFIER
Antibodies		
53BP1	CST	4937S; RRID:AB_10694558
53BP1	BD PharMingen	612522; RRID:AB_2206766
53BP1	NB	NB100-304; RRID:AB_350221
p53	SCBT	sc-126; RRID:AB_628082
CDKN1A/p21	CST	2947S; RRID:AB_823586
MDM2	SCBT	sc-965; RRID:AB_627920
β-Actin	SCBT	sc-47778; RRID:AB_626632
TIRR	Sigma	HPA044186; RRID:AB_10968571
FLAG	sigma	M2 clone-F3165; RRID:AB_259529
GFP	CST	2555; RRID:AB_10692764
p53	Invitrogen	MA5-12571; RRID:AB_10986581
p21	SCBT	sc-756; RRID:AB_2229243
p53K382ac	Abcam	ab75754; RRID:AB_1310532
SET8	CST	2996S; RRID:AB_2254384
USP28	Abcam	ab126604, RRID:AB_11127442
y-H2AX	Millipore	05-636; RRID:AB_309864
Chemicals, peptides, and recombinant proteins		
Nutlin-3	Cayman Chemical	10004372
Dulbecco's modified Eagle medium	GIBCO	11995-065
Penicillin-Streptomycin	GIBCO	15140
RNeasy mini extraction kit	QIAGEN	74104
Superscript iii first strand synthesis system	Invitrogen	18080-051
Power Sybr green master mix	Applied Biosystems	4367659
Flag-M2 agarose beads	Sigma	A2220
GFP-trap	Chromotrek	GTA-20
DAPI	Sigma	D9542
Cycloheximide	Sigma	C7698
MG132	Selleckchem	S2619
Triton	Fisher	AC327371000
Tris-HCL	Invitrogen	15567-027
Glycine	Sigma	G8898
Resazurin	Sigma	R7017
Crystal violet	Millipore	C0775
Dynabeads CD25	Life Technologies	11157D
Pierce ChIP-grade Protein A/G Magnetic Beads	Thermofisher Scientific	26162
Lipofectamine RNAiMAX Transfection Reagent	Invitrogen	13778150
TrueCut Cas9 Protein v2	Thermofisher Scientific	A36497
Lipofectamine 2000	Invitrogen	11668019
MNase enzyme	Thermofisher Scientific	10107921001
Centrinone	Cayman chemicals	CFI-400945
PI/RNase staining buffer	BD biosciences	550825
P53K370me2	Cui et al., 2009	N/A

(*Continued on next page*)

Please cite this article in press as: Parnandi et al., TIRR inhibits the 53BP1-p53 complex to alter cell-fate programs, Molecular Cell (2021), https://doi.org/10.1016/j.molcel.2021.03.039

Continued

REAGENT or RESOURCE	SOURCE	IDENTIFIER
P53k382me2	Cui et al., 2009	N/A
53BP1 TTD	Botuyan et al., 2018	N/A
Critical commercial assays		
Duolink PLA red *in situ* mouse/rabbit starter kit	Sigma	DUO92101
Duolink PLA multi probe reagent kit	Sigma	DUO96000
TaqMan Array Human p53 Signaling	Thermofisher Scientific	4414168
Q5 site directed mutagenesis kit	NEB	E0554S
Beta galactosidase staining kit	CST	9860S
Deposited data		
RNA sequencing data in CT and TIRR KO	This paper	PRJNA661632
Experimental models: Cell lines		
RPE1	ATCC	ATCC® CRL-4000
RPE1 CT	This paper	N/A
RPE1 TIRR −/− #3	This paper	N/A
RPE1 TIRR −/− #5	This paper	N/A
RPE1 53BP1 −/−	Drané et al., 2017	N/A
RPE1 p53 −/−	This paper	N/A
U2OS	ATCC	ATCC® HTB-96
U2OS TIRR −/− #5	This paper	N/A
U2OS TIRR −/− #17	This paper	N/A
Oligonucleotides		
HPRT1, Actin, GAPDH MM	IDT	Housekeeping mastermixes
TP53 sgRNA #1: 1-F: ACCGGCAGTCACAGCACATGACGG	IDT	N/A
TP53 sgRNA #1: 1-R: AAACCCGTCATGTGCTGTGACTGCC	IDT	N/A
TP53 sgRNA #2: 2F:CACCGGCTTGTAGATGGCCATGGCG	IDT	N/A
TP53 sgRNA #2: 2R: AAACCGCCATGGCCATCTACAAGCC	IDT	N/A
TIRR sgRNA: CAGTGCCAAGATGTCGACGG(CGG)	IDT	N/A
53BP1 sgRNA: AGAACGAGGAGACGGUAAUAGUGGG	IDT	N/A
Primers for qRT-PCR, see Table S1	IDT	N/A
Recombinant DNA		
pOZ-FH-N 53BP1 wt (full-length)	Botuyan et al., 2018	N/A
pOZ-FH-N 53BP1 wt (del BRCT)	Drané et al., 2017	N/A
pOZ-FH-N TIRR (WT)	Botuyan et al., 2018; Drané et al., 2017	N/A
pOZ-FH-N TIRR (K10E)	Botuyan et al., 2018; Drané et al., 2017	N/A
pOZ-FH-N TIRR (R107S)	Botuyan et al., 2018	N/A
GFP-p53	Addgene	Addgene plasmid # 12092
GFP-p53 (del CTD)	This paper	N/A
GFP-p53 (K382R)	This paper	N/A
Software and algorithms		
FlowJo	FlowJo	https://www.flowjo.com/
DEseq2	Love et al., 2014	https://github.com/mikelove/DESeq2

(*Continued on next page*)

Please cite this article in press as: Parnandi et al., TIRR inhibits the 53BP1-p53 complex to alter cell-fate programs, Molecular Cell (2021), https://doi.org/10.1016/j.molcel.2021.03.039

Continued

REAGENT or RESOURCE	SOURCE	IDENTIFIER
EdgeR	Robinson et al., 2010	https://bioconductor.org/packages/release/bioc/html/edgeR.html
IPA	QIAGEN	https://digitalinsights.qiagen.com/products/ingenuitypathway-analysis;%20release%202019-06-15/
Modfit	Modfit	http://www.vsh.com/products/mflt/index.asp
Cell Profiler	Cell Profiler	https://cellprofiler.org/
Biorender	Biorender	https://biorender.com/
Rstudio v1.2.1335	Rstudio, Inc.	https://www.rstudio.com/
Graphpad Prism 7	Graphpad	https://www.graphpad.com/scientific-software/prism/

RESOURCE AVAILABILITY

Lead contact

Further requests for reagents and resources should be directed to and will be fulfilled by the lead contact, Dr. Dipanjan Chowdhury (dipanjan_chowdhury@dfci.harvard.edu).

Materials availability

Materials used in this study are available upon reasonable request.

Data and code availability

The accession number for the RNA sequencing data reported in this paper is Bio BioProject: PRJNA661632.

EXPERIMENTAL MODEL AND SUBJECT DETAILS

All RPE1, U2OS, and HEK293T cell lines used in this work were grown in Dulbecco's Modified Eagle's medium supplemented with 10% FBS and 1% penicillin-streptomycin. All cell lines were grown in 37°C and 5% CO2. Cell lines tested negative for mycoplasma.

Gene editing

RPE1 and U2OS TIRR-KO cell lines were generated using the Alt-R CRISPR-Cas9 technology (IDT). CRISPR guides (sgRNAs) were designed using CHOPCHOP and DeskGen CRISPR guide design tools. The RNP complex was generated by first combining 2.4 μl sgRNA (100 μM/L stock) and 2.4 ul tracrRNA (100 μM/L stock) in a PCR tube with 5.2 μl nuclease free water, generating a 240 pmol sgRNA solution. The sgRNA solution was combined by the following PCR reaction: 95°C 5min, 1°C/min decrease to 12°C, then infinite hold at 12°C. Next, 200 pmol Cas9 was combined with 120 pmol sgRNA solution and incubated at room temperature for 10 mins to allow RNP formation. The RNP complexes were introduced into RPE1 cells by electroporation using the Lonza Nucleofector X system. After 72 hours, the knockout cell pools were tested by immunoblotting using relevant antibodies. After confirming a decrease in expression of proteins, single clones were sorted and tested by both immunofluorescence and immunoblotting.

METHOD DETAILS

Retrovirus production

HEK293T cells were transfected with TIRR (WT/K10E/R107S) – pOZ-FH-N constructs and viral packaging plasmids. Retroviral particles were collected after 48 hours and used to infect RPE1 TIRR-KO cells. TIRR-KO cells stably complemented with pOZ-TIRR vectors were selected using magnetic CD25-Dyna beads.

RNAi

p53 ORF siRNA: 5′ ccagtggtaatctactgggacggaa 3′, 53BP1 ORF siRNA: AGAACGAGGAGACGGUAAUAGUGGG, 53BP1 UTR siRNA: AAAUGUGUCUUGUGUGUAA, USP28 siRNA: CUGCAUUCACCUUAUCAUU

10μM siRNA was transfected in cells using Invitrogen Lipofectamine RNAiMAX using the manufacturer's protocol. The medium was changed 24 hours after the transfection. Cells were harvested for RNA and protein extraction after 48 hours.

Please cite this article in press as: Parnandi et al., TIRR inhibits the 53BP1-p53 complex to alter cell-fate programs, Molecular Cell (2021), https://doi.org/10.1016/j.molcel.2021.03.039

RNA extraction and RT-PCR

Total RNA was extracted from cells using RNeasy mini kit (QIAGEN) using the manufacturer's protocol. 1-5 μg of total RNA was used to generate cDNA using SuperScript III First-strand synthesis system (Invitrogen). qPCR was done using the 2X SybrGreen Mastermix (Applied Biosystems) and the relevant primers. All qPCR primers used in the study are listed in the Key resources table.

Immunoprecipitation and western blotting

Whole cells protein extracts were generated using a lysis buffer containing 150 mM NaCl, 20 mM Tris-HCl (pH 7.65), 0.5% NP-40, 5 mM EDTA, 5% glycerol and protease and phosphatase cocktail inhibitors (Roche). 30 μg of lysates measured by Bradford assay were loaded into precast gels (Nu-PAGE Invitrogen, 4%–12%). Immunoprecipitation was carried out by incubating 1 mg of protein lysate with Anti-Flag M2 resin (sigma) or GFP-trap, overnight at 4°C. The following day, the beads were washed [20 mM Tris-HCl (pH 7.65), 150 mM NaCl, 3 mM $MgCl_2$, 10% Glycerol, 0.01% NP-40] and eluted in either glycine or 4x SDS loading buffer. With GFP-trap, proteins were eluted directly in 4x loading buffer.

Proximity ligation assay

Cells were plated at 25% confluency on coverslips placed in 12 well-plates. After 48 hours, cells were treated with 4 μM Nutlin-3 for 4 hours and fixed with 4% paraformaldehyde (PFA) solution for 15 minutes. Cells were permeabilized with 0.5% triton for 5 minutes and washed with TBS solution. The steps of blocking, primary antibody incubation, probe incubation, ligation and amplification were followed according to the manufacturer's protocol. The three-probe PLA assay was done in a similar manner with an additional first step of conjugating primary antibodies to the probes (according to manufacturer's protocols).

Chromatin immunoprecipitation

RPE1 cells were grown in 150 mm dishes and were 90% confluent at the time of treatment with Nutlin-3 and extraction. Cells were either untreated or treated with 4 μM Nutlin-3 for 4 hours after which DNA-protein complexes were crosslinked using 1% formaldehyde for 15 minutes. Crosslinking was terminated by adding 125mM Glycine (pH 3.5). Next, the cells were collected after washing twice with 1X PBS and lysed with Lysis Buffer I (50 mmol/L HEPES-KOH, pH7.4; 140 mmol/L NaCl; 10% glycerol; 0.5% NP-40; 0.25% Triton X-100; protease inhibitors) and incubated at 4°C for 15 minutes on a rocker. Upon centrifugation, the nuclei from the cells were collected and lysed with Lysis Buffer II (10 mMol/L Tris-HCl, pH 8.0; 200 mMol/L NaCl; protease inhibitors) for 10 minutes at 4C. The lysates were then washed thrice with MNase buffer and incubated with MNase enzyme (30U/ul). Following this, the nuclei were further lysed with 10 mMol/L Tris-HCl, pH 8.0; 100 mMol/L NaCl; 1 mMol/L EDTA; 0.5 mMol/L EGTA; 0.1% sodium deoxycholate; 0.5% N-lauroylsarcosine; protease inhibitors). The DNA-protein complexes that were extracted were then ruptured using a sonicator (30 s on 30 s off cycles were used for 15 minutes). Dynabeads-G coupled with either p53 (DO-1) (IgG mouse antibody was used as a control) were used to pull down p53 protein and its DNA targets. The nucleoprotein complex was washed and eluted, and the crosslinking was reversed at 65°C for 16 hours followed by proteinase K and RNase treatment. qPCR with relevant primers (provided in Key resources table) was done.

PI staining and FACS

RPE1 cells were plated at 25% confluency and treated with (1.25, 2.5 μM) of Nutlin-3 for 48 hours. Cells were trypsinized, collected and resuspended in 100% methanol and fixed overnight. Cells were washed with PBS and incubated with Propidium Iodide solution (Thermofisher Scientific) for 30 minutes to measure the DNA content. The cell profiles were recorded by Flow Cytometry and analyzed by Modfit software.

Senescence assay

RPE1 Cells were plated at a low confluency in a 6-well plate and allowed to grow for 6 days. Cells were washed twice with 1X PBS, fixed, and stained using solutions provided with beta-galactosidase staining kit (CST). ANKRD1, EDN1, IL6 RNA transcripts were measured according to the RNA extraction and qPCR protocol provided above.

Cell survival assays

In a 96-well plate, 1000 RPE1 cells were plated per well, for treatment with different concentrations of Nutlin-3. The next day, the cells were treated with serially diluted concentrations ranging from 0-10 uM of Nutlin-3. On the fourth day after the addition of Nutlin-3, the medium was replaced with medium containing Resazurin (1X solution; 100X stock: 0.5g Resazurin salt dissolved in 100 mL of 1X PBS) for 3-4 hours at 37°C. Cell viability was calculated by measuring absorbance at 570-600 nm wavelength using a microplate reader.

Bioinformatics

Copy number, mutation and gene expression data were downloaded from the TCGA invasive breast carcinoma (n = 963) and prostate adenocarcinoma (n = 492) cohorts[1,2]. Samples were filtered for *TP53* mutation status and copy number alterations, to retain wild-type samples. 283 breast cancer samples and 75 prostate cancer samples with wild-type *TP53* status and no copy number changes were analyzed. Expression levels for *TIRR* and selected p53 pathway proteins (indicated in Figure 5C) were obtained as z-scores

Please cite this article in press as: Parnandi et al., TIRR inhibits the 53BP1-p53 complex to alter cell-fate programs, Molecular Cell (2021), https://doi.org/10.1016/j.molcel.2021.03.039

relative to diploid samples available from RNaseq V2 RSEM data. *TIRR* wild-type samples were defined as tumors with a z-score < 0, while *TIRR* amplified samples contained a z-score > 1. Pathway expression was calculated as the average of expression for each p53 pathway member.

Preparation of proteins and peptides for NMR spectroscopy and ITC studies

Human 53BP1-Tudor (residues 1484-1603) was expressed in *E. coli* and purified as previously reported (Botuyan et al., 2006). To prepare the 53BP1-TIRR complex, human 53BP1-Tudor and TIRR were co-expressed in *E. coli* and purified has previously reported (Botuyan et al., 2018). The three p53 peptides (residues 363-389), with replacement of Lys370, Lys382 or both by a cysteine, were expressed in *E. coli* BL21 DE3 cells as a C-terminal fusion to a hexahistidine-GB1 (B1 domain of streptococcal protein G) tag. After purification of the peptides by Nickel-NTA affinity chromatography (QIAGEN) and size exclusion chromatography using a Superdex S75 column (GE Healthcare), the dimethyllysine analogs were installed by reductive cysteine alkylation using ^{13}C-enriched dimethylated 2-chloroethylamine. The modified peptides were then purified by size exclusion chromatography using a Superdex S75 column followed by cleavage of the hexahistidine-GB1 tag. Final purification and separation of the p53 peptides from the hexahistidine-GB1 tag was done by reversed-phase chromatography using a preparative C18 column (Phenomenex). The detailed procedure for preparing peptides harboring methyllysine analogs was previously published (Cui et al., 2009). The p53K370me2 (residues 366-375) and p53K382me2 (residues 377-386) peptides used for ITC were purchased from GenScript and purified by reversed-phase chromatography using a preparative C18 column (Phenomenex).

NMR spectroscopy

The NMR experiments were performed at 25°C using a 700 MHz Bruker Avance III spectrometer equipped with a cryoprobe. The NMR titration data were processed using NMRViewJ (Johnson, 2018) and analyzed using standard approaches (Benirschke et al., 2010). The samples were in 50 mM sodium phosphate buffer, pH 7.5, 300 mM NaCl, 1.5 mM NaN3, 0.3 mM DSS, 10% D_2O and 90% H_2O. The p53 peptides at a concentration of 20 μM for p53K_C370me2 and p53K_C382me2, and 10 μM for p53K_C370me2K_C382me2, were titrated with a stock solution of 53BP3-Tudor at a concentration of 1 mM. Similar molar ratios were prepared for the three p53 peptides mixed with the co-purified 53BP1-Tudor-TIRR complex. For straightforward comparison, the molar ratios were reported with respect to the concentration in dimethyllysine analog.

Isothermal titration calorimetry

The ITC measurements were done at 10°C using a VP-ITC instrument (MicroCal – Malvern Panalytical). 53BP1-Tudor in the calorimeter cell and the p53 peptides in the injection syringe were at concentrations of 20-100 μM and 1-4 mM, respectively in 50 mM Tris/HCl (pH 7.5) and 20 mM NaCl. The titrations were paired with injections of the peptides in buffer solution to determine the heat of dilution. Data were fit with a one-site binding model using Levenberg-Marquardt nonlinear regression in Origin 7.0 (OriginLab).

QIBC

QIBC was performed as described previously (Kilic et al., 2019). Asynchronously growing cells were seeded on sterile 12 mm glass coverslips and allowed to proliferate until they reached a cell density of 70%–90%. They were fixed in 4% formaldehyde for 15 minutes at room temperature, washed once in PBS, permeabilized for 5 minutes at room temperature in 0.2% Triton X-100 (Sigma-Aldrich) in PBS, washed twice in PBS and incubated in blocking solution (filtered DMEM containing 10% FBS and 0.02% Sodium Azide) for 15 minutes at room temperature. Primary antibodies were diluted in blocking solution and incubated for 2h at room temperature. Alexa fluor secondary antibodies (Thermo Fischer Scientific) were diluted 1:500 in blocking solution and incubated at room temperature for 1h. Cells were washed once with PBS and incubated for 10 minutes with DAPI, in PBS at room temperature. Following three washing steps in PBS, coverslips were briefly washed with distilled water and mounted on 5 μl Mowiol-based mounting media (Mowiol 4.88 (Calbiochem) in Glycerol/TRIS). 9-16 images per condition were acquired on an Olympus ScanR high-content screening system (IX83 with a Lumencor SpectraX light engine and a Hamamatsu ORCA-FLASH 4.0 V2 sCMOS camera, 2048 × 2048 pixel of size 6.5 × 6.5 um, 12 bit dynamics) using a UPLSAPO 20x air objective (NA 0.75), and analyzed using the Olympus ScanR Image Analysis software version 3.0.1. A dynamic background correction was applied, and nuclei segmentation was performed using an integrated intensity-based object detection module based on the DAPI signal. Downstream analyses focused on properly detected nuclei containing a 2C-4C DNA content as measured by total and mean DAPI intensities. Nuclear fluorescence intensities were quantified and are depicted as arbitrary units. Color-coded scatterplots of asynchronous cell populations were generated with TIBCO Spotfire data visualization software version 7.0.1. Within one experiment, similar cell numbers were compared for the different conditions.

RNA-seq differential gene expression analysis and pathway analysis

RNA-seq data were preprocessed as follows. First, for each sample Kallisto (Gingrich et al., 2016) (version 0.44.0) was used to pseudoalign paired-end sequencing reads to the transcriptome and produce estimated expression abundance for each transcript. GENCODE (Frankish et al., 2019) (release 29) was used as the reference transcriptome annotation. Next, the tximport R package (Soneson et al., 2015) (version 1.10) was used to aggregate the transcript-level abundance results from all samples and produce the gene-level estimated expression counts. These estimated counts were corrected for a potential bias associated with changes

in average transcript length across samples. Finally, genes were filtered out if they are not expressed in most samples, using a low threshold of counts per million (CPM).

Differential gene expression analysis was performed using the edgeR package (Robinson et al., 2010), and the DESeq2 package (Love et al., 2014). The estimated log-fold-changes of the two algorithms were confirmed to be highly similar. Multiple testing correction to control the false discovery rate (FDR) was performed using the Benjamini-Hochberg procedure on the p values.

Pathway analysis was performed using the Core Analysis of IPA (QIAGEN Inc., https://digitalinsights.qiagen.com/products-overview/discovery-insights-portfolio/analysis-and-visualization/qiagen-ipa/; release 2019-06-15).'' The input data used for IPA were the differentially expressed genes (DEGs) obtained from the edgeR algorithm with an FDR of 0.1%.

QUANTIFICATION AND STATISTICAL ANALYSIS

All statistical analyses were carried out using Graphpad tools. p values for qRT-PCR, ChIP-qPCR experiments were calculated by unpaired t tests. p values for PLA experiments were calculated by Mann-Whitney tests. IC_{50} and p value measurements for cell survival curves were assessed by non-regression curve analysis in Graphpad. Significance was described by the following measurement of p values: p value < 0.0001 (****), p value = 0.0002-0.0001 (***), p value = 0.002-0.0002(**), p value = 0.0332-0.002 (*), p value = 0.1234 (ns).